
Paper XXX: Refer to EasyChair Acceptance Email

Thermal inequalities in Mexico City: Coupling remote sensing, urban morphology and microclimate simulation to analyse urban heat exposure

Abstract

The 2025 Lancet Countdown reports that heat related mortality has risen by 23% since the 1990s and that heat exposure led to 640 billion potential labour hours lost in 2024 (Romanello et al., 2025). This paper examines how extreme heat compounds existing social inequalities in Mexico City and develops an operational pathway for delivering cooling where it yields the greatest social benefit. We integrate a decade of summer satellite observations with block level census indicators to estimate daytime air temperature across the entire city. Results indicate systematic exposure disparities: older adults, disabled residents and households without a car are disproportionately located in hotter blocks, commonly experiencing daytime conditions around 2 to 3 °C above the citywide mean, with particularly pronounced concentrations in eastern and central boroughs.

Moving beyond surface mapping, we test whether thermal exposure aligns with the city's everyday movement structure. By combining street-network configuration (Space Syntax) with built-form descriptors (Space Matrix), we show that high-exposure areas also contain highly connected, heavily traversed corridors. In effect, the pedestrian spines that organise daily access and through-movement frequently coincide with elevated heat burden, while compact districts with limited tree cover and scarce public open space intensify local hotspots.

At the pedestrian scale, microclimate simulations clarify the dominant mechanism of discomfort: radiant load from the sun and heated urban surfaces. Simulations along representative corridors show that mean radiant temperature (T_{mrt}) drives thermal stress during the 10:00 to 14:00 period, and that continuous shade provision (via canopies, tree cover or well designed shelters) can substantially moderate perceived heat even when ambient air temperatures remain high.

The contribution is a screening workflow that translates evidence into implementable targets. By jointly considering demographic vulnerability, local temperature variation and network centrality, the method identifies priority corridors where interventions are likely to protect the most exposed groups and the largest numbers of pedestrians. We specify measurable performance objectives to support delivery and evaluation: shade along most of the 10:00 to 14:00 walking window, cooling refuges at 300 to 500 m intervals, and material and building choices that reduce radiant heating without creating glare. The approach avoids costly citywide microclimate modelling, providing a practical tool for local authorities to diagnose risk rapidly, prioritise socially sensitive and highly trafficked streets, and track progress through outcome focused indicators. Although grounded in Mexico City's high altitude context, the framework is transferable to fast growing cities facing similar heat and equity challenges.

urban heat; thermal exposure; heat inequality; Space Syntax; Mexico City

1. Introduction

Cities are facing a rapid escalation of heat related risks with measurable health, economic and urban consequences. In 2024, multiple indicators reached record highs across the climate system (NASA, 2025; NOAA, 2025; Rohde, 2025; World Meteorological Organization, 2025). Public health and labour evidence underscores the scale of the challenge: the Lancet Countdown reports record heat attributable mortality among older adults and rising productivity losses (Romanello et al., 2025), while International Labour Organization projections anticipate losses equivalent to tens of millions of jobs due to heat stress (International Labour Organization, 2019). The IPCC highlights that cities concentrate exposure and vulnerability while also holding key levers for action, calling for explicitly urban metrics and policies (IPCC, 2022). The World Health Organization similarly emphasises the growing burden of heat related mortality and the need for robust, up to date heat and health action plans (World Health Organization, 2024).

Mexico City provides a critical case where intense urban heat intersects with entrenched socio-spatial inequalities. Three practical gaps motivate this research: (i) identifying where exposure concentrates and which groups are most affected; (ii) explaining which features of built form and street-network structure sustain these patterns; and (iii) translating diagnosis into verifiable, performance-based passive design targets. Addressing these gaps requires a shift from descriptive mapping to operational delivery.

The study adopts locally relevant daytime summer air temperature thresholds for risk communication at block scale ($T_a \geq 26^\circ\text{C}$) (Magaña and Vargas, 2020). For outdoor comfort, however, pedestrian thermal load is governed primarily by mean radiant temperature (T_{mrt}), motivating biometeorological indices such as the Universal Thermal Climate Index (UTCI) and Physiological Equivalent Temperature (PET) (Höppe, 1999; Lindberg et al., 2008; Bröde et al., 2012; Jendritzky et al., 2012). Spatial configuration is measured using Space Syntax indicators of integration and choice, normalised as NAIN and NACH, while morphology is described with Space Matrix metrics (Floor Space Index, Ground Space Index, and Open Space Ratio) linking density, accessibility and microclimate (Hillier and Hanson, 1984; Hillier et al., 2012; Berghauser Pont and Haupt, 2020).

The study addresses three research questions:

- **Q1.** Where, and to what extent, do daytime summer mean air temperatures at block level co-locate with socially and physiologically vulnerable groups in Mexico City, and how heterogeneous across municipalities are these associations under thresholds of 26°C or more?
- **Q2.** Which combinations of urban form and density, and network configuration, best characterise thermal and social hotspots, and which contiguous clusters jointly maximise thermal severity and pedestrian accessibility for passive cooling simulation?
- **Q3.** In highly integrated, strongly exposed pedestrian corridors, how can micro scale thermal stress, together with geometric parameters, be assessed to define passive design targets capable of reducing heat?

These questions form a logical chain: Q1 establishes *where* and *for whom* interventions should be prioritised; Q2 explains *why* hotspots persist (form and network mechanisms) and identifies actionable clusters; and Q3 specifies *how much* cooling is needed, and *how* it can be delivered, through verifiable targets.

Methodologically, the paper proposes a city to street pipeline: (i) calibrating satellite derived thermal surfaces with local observations to estimate daytime air temperature (T_a); (ii) overlaying thermal exposure with social sensitivity to identify conservative hotspots; (iii) characterising hotspots with Space Matrix and Space Syntax to locate contiguous clusters that combine thermal severity with high pedestrian accessibility; and (iv) simulating biometeorological indices at micro scale in highly integrated corridors to define passive design targets (continuous shade, non glare cool materials, ventilation). This responds to IPCC and WHO calls to move from generic action lists towards performance oriented delivery with iterative learning and equity (IPCC, 2022; World Health Organization, 2024).

The analysis uses the census block as the unit of analysis, drawing on data from the National Institute of Statistics and Geography (INEGI, 2021) and focusing on the summer period 2014 to 2024 (1 June to 30 August). T_a is calibrated from Land Surface Temperature (LST) using observations from the Mexico City Automatic Weather Station Network (10:00 to 14:00), and air temperature Urban Heat Island (UHI) surfaces are derived in Google Earth Engine (Gorelick et al., 2017). Morphology is drawn from Google Open Buildings and cadastral data, and network configuration is computed from a segmented graph with

NAIN and NACH at radii of 500, 1,000, 1,500 and 5,000 m. Limitations include emissivity and humidity uncertainty, the exclusion of anthropogenic heat in SOLWEIG (Lindberg et al., 2008), and potential topological biases; nonetheless, triangulation across scales (macro, meso and micro) yields a consistent picture.

2. Theory

Urban heat is increasingly recognised as a central public health and planning challenge, with impacts that fall unevenly across social groups (Romanello et al., 2025; World Meteorological Organization, 2025). Two conceptual distinctions are important for interpreting evidence and specifying policy responses. First, the Urban Heat Island (UHI) denotes relative thermal contrasts between urban and rural contexts that arise from materials, morphology and land cover, whereas extreme heat refers to absolute hazardous conditions. The two are related, but not interchangeable, and conflating them obscures risk thresholds and intervention priorities (Stewart and Oke, 2012; IPCC, 2022). Second, heat risk reduction requires locally grounded evidence and institutions that can act on the city scale determinants of exposure, including shade, materials, vegetation and ventilation, rather than relying solely on national aggregates (World Health Organization, 2024). In line with Latin American disaster risk scholarship, heat risk is produced through exposure, sensitivity and adaptive capacity, and is therefore tractable within municipal mandates (Lavell, 1999, 2003).

The literature has shifted from surface proxies towards metrics that better represent lived exposure. Daytime land surface temperature can be only weakly related to near surface air temperature and experienced heat stress within cities (Chakraborty et al., 2022). Because radiative load at pedestrian height governs much of the outdoor thermal experience, assessment increasingly relies on biometeorological metrics, including mean radiant temperature (Tmrt) and UTCI, rather than LST alone. Tools such as SOLWEIG within UMEP for QGIS enable estimates of Tmrt under alternative shading and material scenarios, supporting analyses that are suitable for policy while remaining sensitive to street level conditions (Lindberg et al., 2008, 2018).

In parallel, a substantial equity literature documents systematic disparities in urban heat exposure. The IPCC framing of vulnerability has supported fine grained empirical analyses across age, income and ethnicity. In the United States, historically redlined neighbourhoods are measurably hotter today (Hoffman et al., 2020), and nationwide evidence shows persistent disparities by race and income (Hsu et al., 2021). In Greater London, socio-demographic inequalities align closely with UHI intensity (Krenz and Amann, 2025). Together, these findings motivate multidimensional vulnerability indicators at fine spatial scales and the integration of social datasets with physical exposure layers (IPCC, 2022).

Building on these insights, an emerging strand treats urban form and networks as thermal infrastructures. Space Syntax provides measures that capture how spatial configuration shapes pedestrian flows. Angular analyses identify least angle paths that often predict movement more robustly than metric distance. Core indicators, integration for accessibility and choice for through movement, highlight corridors where flows concentrate and, in the absence of shade, so does thermal burden (Hillier and Hanson, 1984; Hillier et al., 2012). Space Matrix conceptualises density as relational, combining FSI, GSI, L and OSR to position built form within a continuous morphological state space. Compact, high coverage fabrics tend to store heat and suppress evapotranspiration, while more porous forms can promote midday shading and airflow (Berghauer Pont and Haupt, 2020). Read together, these frameworks distinguish structural heat rooted in sealing and vegetation deficits from corridor heat concentrated along highly accessible pedestrian axes.

Mexico City's basin dynamics make the coupling between form, networks and heat particularly salient. Weak synoptic forcing, gap winds and topographic channelling produce shifting ventilation corridors (de Foy et al., 2006a,b), and classic urban climate studies document both the magnitude and spatial patterning of the city's UHI (Jáuregui, 1997). Regional climate work further emphasises the importance of characterising warm spells within their local hydroclimatic context (Magaña and Vargas, 2020). This supports the coupling of calibrated air temperature surfaces with configurational analysis to identify where people walk, dwell and queue during the hottest parts of the day.

Policy practice is beginning to align with this evidence base, yet an evaluation gap remains. Bangkok's heat action initiatives articulate quantified levers but often underspecify how to deliver verifiable reductions in street level Tmrt (World Bank, 2025). Singapore's Cooling Singapore provides a more operational template by targeting the physical determinants of outdoor comfort (ETH Zürich and Singapore, 2017).

In Mexico City, the Climate Action Programme 2021 to 2030 acknowledges heat risks, but measurable corridor level cooling targets remain limited (SEDEMA, 2021). The IPCC notes that poorly specified measures can lead to maladaptation if trade offs are not assessed explicitly (IPCC, 2022).

In synthesis, the literature supports a shift from surface proxies to lived exposure, from citywide averages to block and corridor scale analysis, and from generic checklists to interventions that can be monitored against measurable outcomes. The methodological gap addressed here concerns integration: linking social vulnerability with configurational (Space Syntax) and morphological (Space Matrix) analysis, and evaluating passive measures against biometeorological metrics along the pedestrian networks where exposure concentrates (Lavell, 1999; IPCC, 2022).

3. Datasets and Methods

This section summarises the datasets and analytical workflow used to assess urban heat exposure in Mexico City and its relationship to urban form and social vulnerability. The approach is organised across three nested spatial scales (macro, meso, and micro), enabling a progressive transition from citywide screening to street level simulation.

Table 1 Data sources and derived inputs by methodological step.

Step	Raw data sources (and key derived inputs)
<i>Abbrev.: L8/9 = Landsat 8/9; GEE = Google Earth Engine; LST = Land Surface Temperature; Ta = air temperature; DEM/DSM = Digital Elevation/Surface Model; GOB = Google Open Buildings; OSM = OpenStreetMap; INEGI = Instituto Nacional de Estadística y Geografía.</i>	
Macro scale: thermal mapping + vulnerability co-location	
1.1	Landsat 8/9 Collection 2 Level 2 products (surface reflectance + LST), summer scenes (1 June to 30 August, 2014 to 2024) processed in GEE; derived indices: NDVI, NDBI, short wave albedo
1.2	Meteorological stations (RedMet; hourly observations between 10:00 and 14:00) to calibrate LST to Ta; derived: Ta surface (30 m) and thermal thresholds (hot26/hot28)
1.3	INEGI 2020 Census microdata at block (manzana) level; indicators: 65+, ages 6 to 14, disability, households without a car, no health services, economic inactivity, incomplete primary education; derived local models (GWR/MGWR) and thermal and social hotspots
Meso scale: urban morphology + street network configuration	
2.1	Building footprints and heights (GOB v3; complemented with cadastral floor area where available); derived Space Matrix indicators (FSI, GSI, OSR, L) and typological labels
2.2	Street network (OSM) modelled as a segment graph; derived Space Syntax metrics (NAIN/NACH; DepthmapX) at 500, 1,000, 1,500, and 5,000 m
2.3	Coupling dataset joining hotspot blocks/adjacent segments with Ta and form/network metrics; derived corridor candidates (hot + integrated) for micro-scale case studies
Micro scale: biometeorological simulation (pedestrian exposure)	
3.1	High-resolution DEM/DSM (INEGI 1:10,000), building footprints/heights (Step 2.1), and canopy/vegetation layers (NDVI-derived); derived radiative parameters (SVF, wall heights/aspects)
3.2	UMEP/SOLWEIG in QGIS with local meteorological forcing; simulations at 10:00, 12:00 and 14:00; derived pedestrian exposure metrics along selected corridors: Tmrt, UTCI, PET

3.1. Urban Thermal Mapping: Satellite to Ground Calibration

Level 2 Landsat 8/9 summer imagery (1 June to 30 August, 2014 to 2024) was processed in Google Earth Engine using standard scaling and cloud and cirrus masking (Gorelick et al., 2017). Land surface temperature was retrieved with an emissivity correction based on NDVI derived vegetation fraction, and NDVI, NDBI, and short wave broadband albedo were computed from surface reflectances (Tucker, 1979; Zha et al., 2003; Liang, 2001).

To reflect Mexico City's high altitude and typically low humidity, LST was empirically converted to air temperature using hourly RedMet observations between 10:00 and 14:00 from 18 stations. A city specific transfer function ($Ta = 0.5540 \times LST + 5.7606$) was applied to all scenes, addressing known LST to Ta discrepancies and acknowledging the role of humidity in experienced heat stress (Chakraborty et al., 2022). Annual summer medians were then averaged to produce a 2014 to 2024 climatology. From the calibrated Ta fields we derived UHI_air (z-scores of Ta) and UTFVI_air (Waleed et al., 2023). Outputs are provided at 30 m resolution and serve as inputs across all subsequent analytical steps.

3.2. Socio-demographic Indicators

Socio-demographic indicators were drawn from the 2020 Mexican Population and Housing Census at the urban block (manzana) level (INEGI, 2021). Indicators were operationalised as block level percentages or ratios using official denominators, with selection guided by physiological sensitivity and exposure constraints (Table 1).

3.3. Urban Morphology: Space Matrix

Urban morphology was described at the block level using the Space Matrix framework (Berghauser Pont and Haupt, 2020). Building footprints were obtained from Google Open Buildings and combined with cadastral information on built floor area to compute four indicators: Floor Space Index (FSI), Ground Space Index (GSI), equivalent number of floors (L), and Open Space Ratio (OSR) (Google Research, 2023). In Space Matrix terms, FSI captures built intensity, GSI captures ground coverage, L captures average storeys as a relation between intensity and coverage, and OSR represents the amount of open ground space per unit of gross floor area (Berghauser Pont and Haupt, 2020, p. 94 to 97).

Although Space Matrix is continuous, we applied typological labels for cartographic interpretation by classifying blocks using thresholds in FSI, GSI and L. The resulting classes include Open Pavilions, Row/Attached low rise housing, Low to Dense Perimeter blocks, Linear Bars, Towers in a Park, Super compact high rises, Compact low rise fabrics, and Mixed/Indeterminate forms.

3.4. Network Configuration: Space Syntax

The street network was modelled as a segment graph and analysed using angular centralities across multiple radii to capture connectivity from local to metropolitan scales. Angular analysis treats changes of direction as the cost of shortest paths and has repeatedly been shown to predict movement more robustly than purely metric distance (Hillier and Hanson, 1984; Hillier et al., 2012). To support comparison across systems, we report the normalised measures of integration and choice.

Normalised Angular Integration (NAIN) adjusts angular total depth by benchmarking each segment against system averages, yielding values that are less sensitive to graph size. Normalised Angular Choice (NACH) addresses the tendency for segregated configurations to inflate raw choice values by dividing choice by depth, framing through movement in cost benefit terms (Hillier et al., 2012). Both normalisations reflect the broader Space Syntax objective of reducing graph size effects so that depth and choice can be compared across systems.

Together, NAIN and NACH allow integration and choice to be compared across radii, systems, and study areas, providing a consistent basis for examining spatial accessibility and segregation in the street network.

NAIN and NACH were computed at 500 m, 1,000 m, 1,500 m, and 5,000 m. These radii bracket immediate pedestrian reach (~500 m), neighbourhood spans (~1 to 1.5 km), and interzonal structure (~5 km) widely used in angular analyses. Although statistical analyses were restricted to census blocks inside the administrative boundary, the segment map was constructed with a 10 km buffer around the urbanised area to minimise edge effects. Pre-processing in QGIS and DepthmapX included topological simplification; segment centralities were exported and area-weighted to blocks for integration with other layers.

Decadal thermal layers (Landsat-derived, emissivity-corrected LST calibrated to air temperature, Ta mean) were sampled within 10-m buffers along segments to attach mean and maximum thermal attributes. Thermalised centralities were then defined by penalising least-angle paths traversing hot segments. Using local public-health thresholds, segments were classified into heat-exposure categories: Baseline (Ta mean < 26°C), Hazardous (26°C ≤ Ta mean < 28°C), and Extreme (Ta mean ≥ 28°C) (Magaña and Vargas, 2020).

3.5. Scales of Analysis

This subsection summarises modelling choices by scale.

Macro scale. Summer daytime air temperature per block is obtained by applying the city specific transfer function from LST to Ta. GWR models are estimated by borough (adaptive bandwidth, bisquare

kernel) to capture spatial heterogeneity in associations between heat and the socio-demographic indicators described above. Hotspots are defined conservatively as blocks that exceed an absolute thermal threshold and display at least one positive, statistically significant local association.

Meso scale. For hotspot blocks, morphology and configuration are coupled by joining Space Matrix indicators and Space Syntax metrics to adjacent street segments. Adjacent segments (15 m buffer) are aggregated using length weighted means and p90, and the shares of segment length falling into $26 \leq Ta < 28$ and $\geq 28^{\circ}C$ are recorded. This supports the selection of contiguous, representative clusters by typology and high accessibility, with emphasis on 500 to 1,500 m radii, for micro scale simulation.

Micro scale. Selected corridors are simulated with UMEP/SOLWEIG in QGIS (Lindberg et al., 2018). Input datasets (Table 1) are harmonised to a 1 m grid to derive SVF, wall heights and aspects for radiative exchange within street canyons (Lindberg et al., 2018).

Across three study areas (Hospital General, Airport, and Basílica), SOLWEIG simulations were run at 10:00, 12:00 and 14:00 to estimate mean radiant temperature (Tmrt) and derive UTCI and PET (Lindberg et al., 2008; Lindberg and Grimmond, 2011; Lindberg et al., 2018).

UTCI (UTCI-Fiala) and PET (MEMI) were computed as equivalent temperature indices that integrate air temperature, wind, humidity and radiation to assess pedestrian thermal stress (Bröde et al., 2012; Jendritzky et al., 2012; Matzarakis et al., 1999, 2007).

Observation points (POI) were placed along high integration corridors identified with Space Syntax (DepthmapX) using NAIN at $r = 500$ m and $r = 1,500$ m (local and neighbourhood scales). High integration at both radii was used to select “robust spines”, streets that are important both locally and for through movement.

Hourly outputs were extracted at POI and summarised across zones (means and 14:00 severity ranks). These outputs were cross-referenced with Space Matrix typologies and thermal and social vulnerability (GWR) under hot26 and hot28 to identify convergence between radiative peaks, integrated corridors and social sensitivity.

Note: Figure 1 summarises the three-scale workflow, and Table 1 lists the data sources used at each step. Modelling choices that are not evident from the schematic are detailed above.

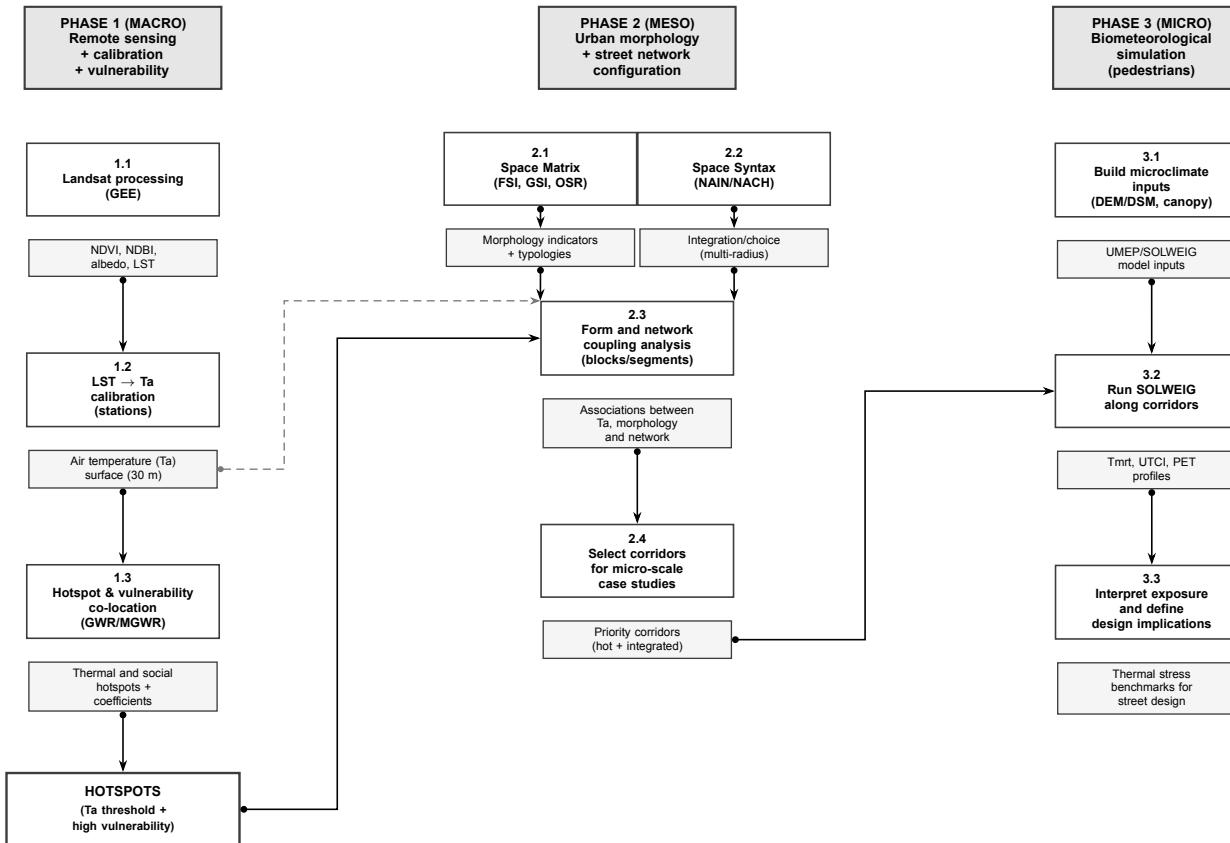


Figure 1 Three-scale methodology linking macro screening (thermal and social hotspots), meso characterisation (form and network), and micro simulation (pedestrian thermal stress).

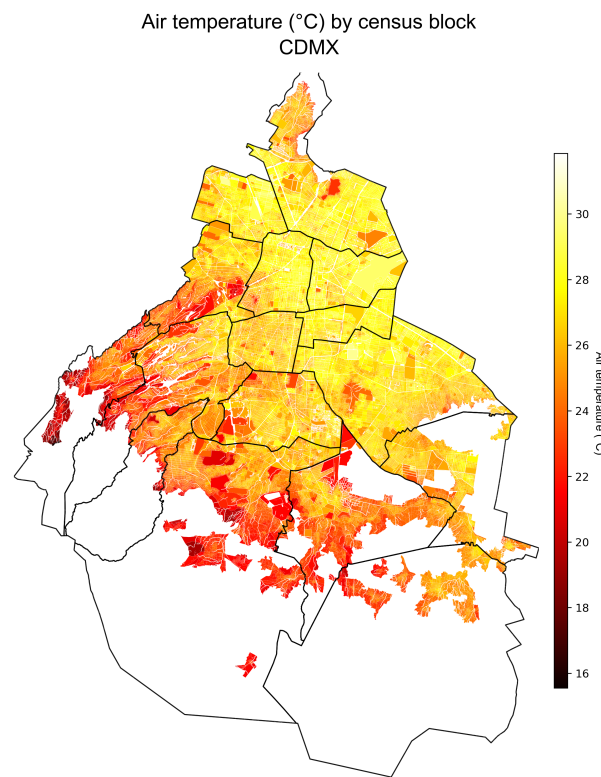
4. Results

4.1. Macro Scale: Urban Heat Island and Socio-demographic Vulnerability

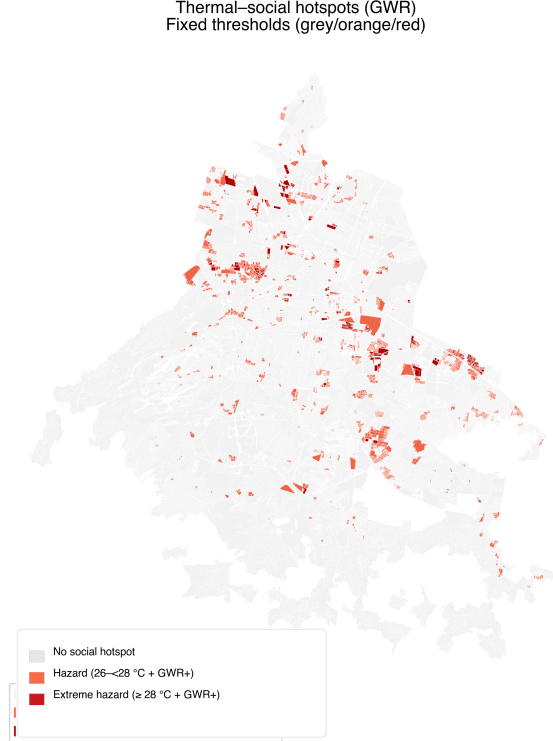
The decadal summer climatology shows a pronounced thermal gradient across Mexico City that is consistent with the urban heat island (UHI). Average near surface air temperatures, calibrated from Landsat land surface temperature (LST) using the RedMet regression, reach approximately 26.8°C in central and eastern boroughs including Cuauhtémoc, Benito Juárez, Iztacalco, Venustiano Carranza and Iztapalapa. Peripheral areas with higher elevations and more vegetation, notably Xochimilco, Milpa Alta and the Ajusco foothills in Tlalpan, register lower summer means of 23 to 24°C. The pattern is consistent with dense built form and limited vegetation amplifying heat in the urban core, while conservation land and montane forests provide cooling at the basin edges.

Complementary indices highlight the spatial concentration of thermal stress. UHI intensity (UHI_air), expressed as the z-score of calibrated air temperature, exceeds $+1.5\sigma$ in the east and northeast, especially in Iztapalapa, Gustavo A. Madero and Venustiano Carranza. These boroughs combine compact housing, industrial corridors and limited vegetation cover, and they coincide with the most severe exposure. Spectral indicators reinforce the interpretation: blocks with NDVI below 0.2 and NDBI above 0.4 repeatedly align with hotspots, while slightly higher albedo in lower density western boroughs moderates localised heating.

Applying locally relevant daytime thresholds (26°C risk; 28°C extreme) (Magaña and Vargas, 2020) underscores the scale of exposure. Approximately 32% of census blocks exceed 26°C, and 11% surpass 28°C in the summer mean. The concentration of these extremes in the centre and east indicates a structural inequality: the densest and most transit dependent boroughs are also those where residents experience the highest outdoor heat burden.



(a) Calibrated summer daytime air temperature (Ta) by census block.



(b) Thermal and social hotspots from GWR under fixed thresholds (26 to <28 $^{\circ}\text{C}$; \geq 28 $^{\circ}\text{C}$).

Figure 2 Macro scale thermal exposure and thermal and social hotspots across Mexico City. All maps are oriented with north at the top.

Socio-demographic indicators are spatially uneven, with potentially vulnerable groups clustering in specific areas. Children are more prevalent in peripheral boroughs with weaker infrastructure and fewer urban services. Older adults are more common in semi-rural and southern boroughs, where health service provision and socioeconomic conditions are often more constrained. People with disabilities, around five percent of the population, are distributed across the city, yet face mobility and accessibility barriers that can heighten exposure.

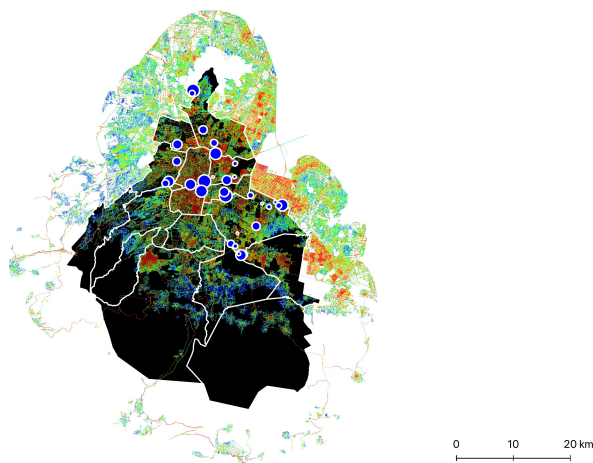
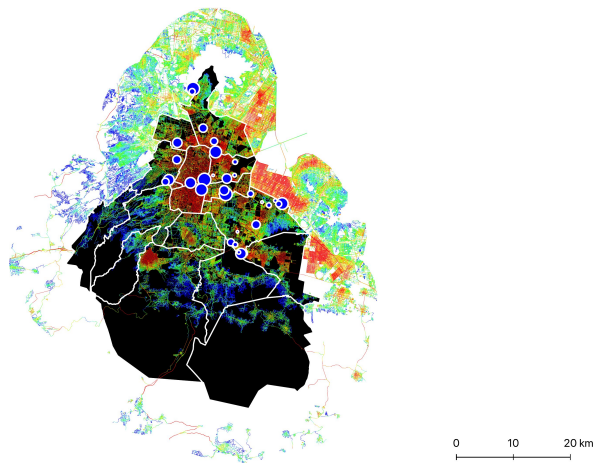
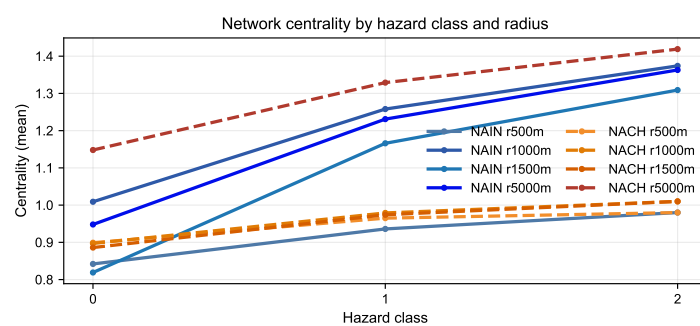
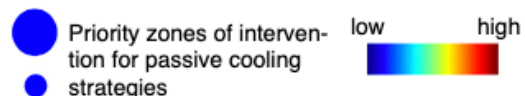
Spatial co location (bivariate LISA) identifies high concentration clusters in eastern and central boroughs, while low concentration clusters are concentrated in southern and peri urban zones. Consistent with these patterns, the central eastern corridor, spanning Iztapalapa, Venustiano Carranza, Gustavo A. Madero and the eastern part of Cuauhtémoc, emerges as a persistent hotspot belt.

GWR results indicate that socio-demographic associations with Ta_mean vary across the city. The share of older adults (65+) shows consistently positive local associations, especially in Milpa Alta, Xochimilco and Tláhuac, where ageing populations coincide with weaker health infrastructure, while effects in central boroughs are weaker or insignificant. Children aged 6 to 14 show smaller and more variable relationships, with significance limited to parts of Iztapalapa and Gustavo A. Madero. Disability is relevant in several southern and eastern boroughs where accessibility barriers are common. Car absence shows modest overall effects but becomes significant in peripheral areas where long public transport commutes may intensify exposure.

Eastern and southern boroughs, particularly Iztapalapa, Tláhuac, Milpa Alta, Xochimilco and Magdalena Contreras, accumulate the largest and most significant coefficients across multiple variables. Central boroughs such as Benito Juárez, Cuauhtémoc and Miguel Hidalgo show weaker or non significant associations. The geography points to a need for place sensitive intervention design that recognises how social structure and territorial inequality shape heat exposure.

4.2. Macro Scale: Network Analysis

Across the radii considered, integration (NAIN) declines as radius expands, while choice (NACH) remains comparatively stable. This scale sensitivity suggests that local positional advantage varies more strongly than route diversity. Importantly, the hazard ranking is consistent at all radii: hotter areas (Hazard 2) show the highest integration and choice, followed by intermediate areas (Hazard 1), with cooler areas (Hazard 0) consistently lowest.

(a) NAIN, $r = 500$ m (walkable scale).(b) NAIN, $r = 1,500$ m (neighbourhood scale).

(c) Network centrality by hazard class and radius (mean values).

Figure 3 Space Syntax integration (NAIN) at two radii used to characterise pedestrian accessibility across the network, alongside centrality profiles by hazard class.

At 5 km, NAIN reaches 1.31 in Hazard 2 and 1.17 in Hazard 1, compared with 0.82 in Hazard 0. NACH is 0.98 in Hazard 2 and 0.94 in Hazard 1, both higher than 0.84 in Hazard 0. Heat exposed zones are therefore also zones of stronger integration and route choice, indicating that accessibility can reinforce thermal vulnerability at this intermediate scale.

Correlation analysis supports the same interpretation. Mean air temperature is positively associated with integration, and the association strengthens with radius, from $r = 0.105$ at 500 m to $r = 0.285$ at 5 km. Hazard 2 zones both concentrate higher integration values and retain this advantage as scale widens, suggesting structural configurational benefits that coincide with elevated thermal stress. Hazard 1 areas occupy an intermediate position, with integration above the city average and clearly above Hazard 0, but below the extremes in Hazard 2. NDVI shows the expected negative association with integration, with the strongest signal again in Hazard 2 where built form intensity and network centrality coincide with reduced greenness.

4.3. Meso Scale: Form and Network Coupling

The meso scale analysis examines how configurational accessibility (Space Syntax) and morphological form (Space Matrix and typological profiles) combine to structure heat exposure. Although Space Syntax is often deployed at metropolitan scales, here centralities are interpreted as meso scale indicators of neighbourhood accessibility, enabling closer linkage between morphological conditions and thermal outcomes.

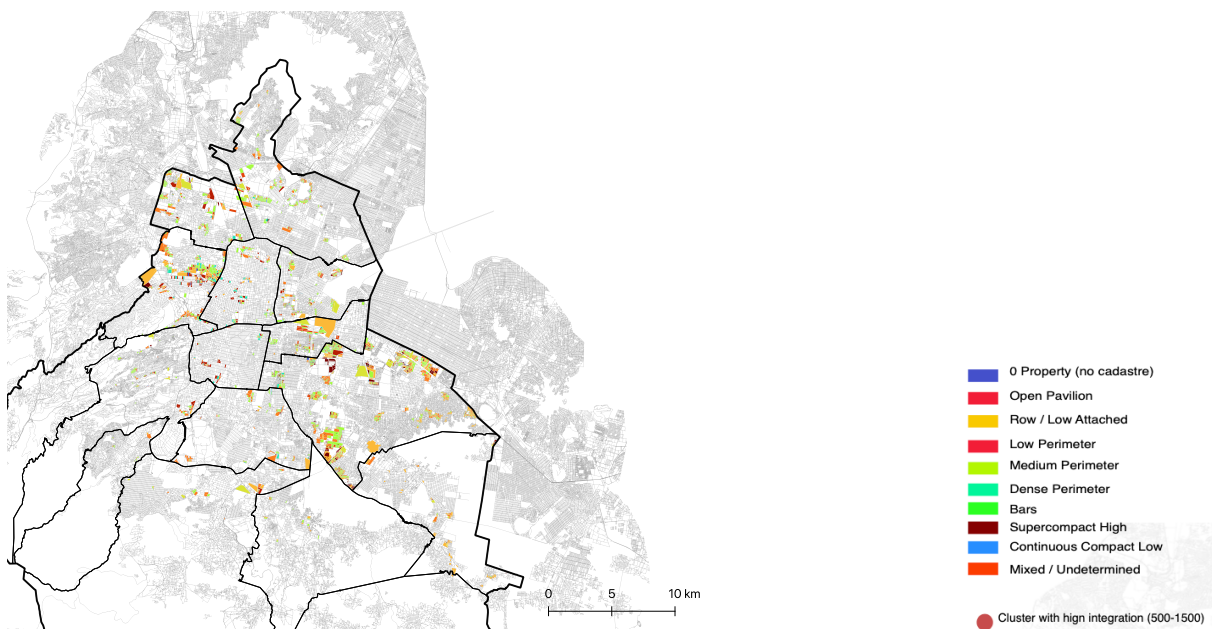


Figure 4 Meso-scale morphology context (Space Matrix typologies) used to interpret thermal hotspots and corridor selection.

Space Matrix results reinforce this picture. Ground Space Index (GSI) is negatively correlated with NDVI ($r = -0.299$) and positively associated with Ta_mean ($r = 0.228$). Typology level exposure patterns and the resulting heat index are summarised in Table 2, where Dense Perimeter and Continuous Compact Low show the highest values and transitional typologies remain elevated.

Typology Code	Typology Name	n	n_hot2	n_hot1	pct_hot2	pct_hot1	Heat Index
OP	0 Property (no cadastre)	1558	489	1069	0.314	0.686	1.314
0	No data	58	9	49	0.155	0.845	1.155
1	Open Pavilion	72	7	65	0.097	0.903	1.097
2	Row / Low Attached	505	41	464	0.081	0.919	1.081
3	Low Perimeter	1410	111	1299	0.079	0.921	1.079
4	Medium Perimeter	125	13	112	0.104	0.896	1.104
5	Dense Perimeter	70	15	55	0.214	0.786	1.214
6	Bars	179	10	169	0.056	0.944	1.056
8	Supercompact High	56	6	50	0.107	0.893	1.107
9	Continuous Compact Low	250	47	203	0.188	0.812	1.188

Table 2 Heat exposure by Space Matrix typology (hot classes and heat index).

Taken together, the evidence indicates that Hazard 1 and Hazard 2 areas are not only hotter, but also structurally advantaged in accessibility terms. Hazard 2 zones retain positional and configurational advantages across scales, combining mobility and centrality benefits with elevated thermal risk. Hazard 1 zones are transitional: they share many spatial advantages of Hazard 2, but with lower heat loads, making them plausible candidates for early mitigation. Hazard 0 zones are comparatively peripheral both thermally and configurationally, combining lower exposure with lower accessibility.

Overall, the meso scale results show that the hottest parts of the city are also the most integrated, and the overlap strengthens as analysis radius expands. Morphology confirms that dense, sealed typologies dominate Hazard 2, while Hazard 1 mixes compact and transitional forms that still show elevated Heat Index values. The convergence of configurational advantage and thermal vulnerability provides a clear basis for targeted interventions. Hazard 2 zones require urgent mitigation through shade, careful use of reflective materials, and greening that preserves network legibility. Hazard 1 areas require a balance of permeability and microclimate measures to prevent progression into the highest risk category.

Priority zones were identified by combining morphological typologies with accessibility metrics. Typologies were ranked by thermal severity using the share of blocks classified as danger (26 to $<28^{\circ}\text{C}$) and extreme danger ($\geq 28^{\circ}\text{C}$), and a composite heat index was computed. Within the most exposed typologies, blocks with the highest configurational accessibility (NAIN and NACH at 500 m and 1,500 m) were selected, with greater weight given to the pedestrian scale due to its relevance for everyday exposure. Selected blocks were then aggregated into contiguous zones using minimum thresholds for spatial continuity and size, yielding robust clusters for micro scale analysis.

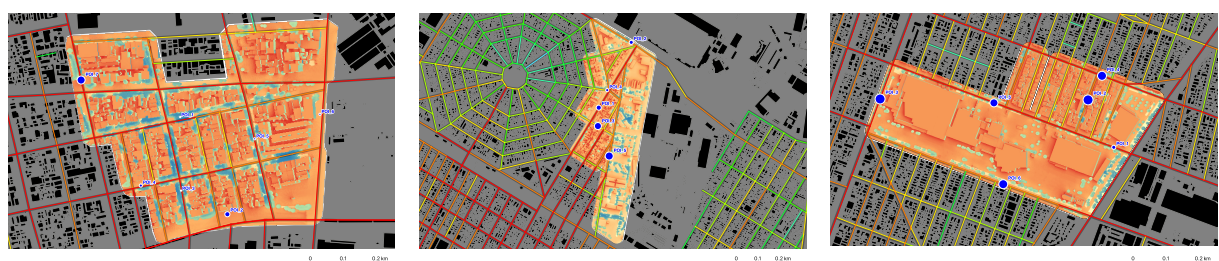
4.4. Micro Scale: Biometeorological Simulations

At the micro scale, pedestrian heat stress was evaluated with UMEP/SOLWEIG using zone specific air temperature and humidity forcing, with Tmrt, UTCI and PET computed at 10:00, 12:00 and 14:00. Observation points were placed on highly integrated pedestrian corridors (NAIN at radii 500 and 1,500 m) to sample locations where exposure is most likely. Under Mexico City's high irradiance conditions, Tmrt maxima occur on open horizontal surfaces at pedestrian level, including plazas, car parks and wide roads, rather than on rooftops when assessed at 1.5 m height. The pattern reflects the city's latitude (approximately 19°N), which yields near zenith solar elevations and short midday shadows, and its high altitude (approximately 2,240 m a.s.l.), which reduces optical air mass and often coincides with dry, transparent air. Together these factors intensify sun and shade contrasts and long wave emission from heated pavements towards pedestrians (Lindberg et al., 2008; Lindberg and Grimmond, 2011).

To support comparison across corridors, we report micro scale results at 14:00 as a conservative reference time. Across the three zones, 14:00 coincides with high solar elevation and accumulated surface heating, and it consistently produces the highest or near highest Tmrt and PET values at the observation points. This time step therefore captures the period when shade deficits translate most directly into pedestrian risk, and it provides a stable basis for ranking corridors and testing design options. Although some locations show short lived peaks earlier, the 14:00 fields summarise severe conditions that persist across the late morning and early afternoon window.



(a) Case study locations (1 to 3) across Mexico City.



(b) Case 1 (Hospital General): (c) Case 2 (Airport): Tmrt at 14:00. (d) Case 3 (Basílica): Tmrt at 14:00.

Figure 5 Micro-scale case studies and peak-stress snapshot (14:00) used for cross-case comparison of pedestrian thermal exposure.

Case 1: Hospital General. Around Hospital General, vulnerability is linked primarily to the 26 to 28°C band. The GWR results indicate that every block exhibited at least one social factor associated with thermal hazard. Associations were most consistent for low educational attainment (primary education; 16/16 blocks) and the 65+ population (8/16), indicating high sensitivity under moderate heat. Other factors, including children aged 6 to 14 and lack of medical services, appear less frequently, and no associations are observed under the extreme threshold ($\geq 28^\circ\text{C}$).

These social patterns align with the local urban fabric, which is dominated by Low Perimeter (37.5%), Bars (31.2%) and Medium Perimeter (25.0%) forms. All typologies fall within hot26, with no hot28 presence, and every type exhibits significant GWR associations at the moderate threshold.

Microclimate simulations corroborate the escalation of stress across the day. UTCI increases from 29.6°C at 10:00 (moderate stress) to 32.9°C at 14:00 (strong stress), while PET reaches 37.2°C on average by 14:00, with several locations above 41°C (very strong). The increase is driven by mean radiant temperature (Tmrt), which rises from 42.7°C to 55.0°C and is strongly correlated with PET and UTCI. The most severe points, including POI 7 and POI 2, occur along highly integrated pedestrian corridors, illustrating how perimeter morphologies embedded within accessible networks can intensify exposure for socially sensitive groups.

Case 2: Airport. Around Benito Juárez International Airport, vulnerability takes a different form. Low educational attainment is the only factor consistently associated with heat, appearing in 22/24 blocks at 26 to 28°C and in 2/24 blocks at $\geq 28^\circ\text{C}$. Other groups, including older adults and children, show no significant associations. Vulnerability in this area is therefore concentrated in educational disadvantage rather than demographic structure.

The Space Matrix composition reflects this context. More than half of the area is classified as 0 Property/no cadastre (54.2%), with a further 29.2% Low Perimeter and smaller shares of Row/Attached (8.3%), Mixed (4.2%) and Open Pavilion (4.2%). While most forms remain within hot26, Low Perimeter and Row/Attached already show a shift towards hot28 (14.3% and 50% of stock, respectively), with GWR coupling mirroring the higher threshold. Zone 2 therefore functions as a transition area where typologies begin to express vulnerability under $\geq 28^\circ\text{C}$.

Thermal simulations indicate sustained stress. UTCI remains around 34 to 35°C and PET varies between 38.7 and 40.8°C, with peaks above 41°C at 10:00 and 14:00. Tmrt exceeds 63°C at these times, explaining the intensity of exposure. The most critical conditions occur on high integration corridors, especially around POI 3, POI 1 and POI 5 where PET exceeds 42°C. Educational disadvantage and typologies transitioning towards hot28 therefore coincide with the busiest, most integrated routes, amplifying risk for local pedestrians.

Case 3: Basílica de Guadalupe. Around the Basílica de Guadalupe, vulnerability emerges primarily under extreme heat ($\geq 28^\circ\text{C}$). At this threshold, 8/9 blocks show significant associations, largely driven by older adults (65+; 6/9), with isolated links to children (1/9) and low education (1/9). At 26 to 28°C, only 1 block shows any association. Vulnerability here therefore becomes salient mainly once temperatures exceed 28°C, with older adults as the principal at risk group.

This pattern is underpinned by morphology. The area is dominated by Continuous Compact (44.4%) and Low Perimeter (33.3%) forms, with Row/Attached comprising the remainder (22.2%). Compact and perimeter types sit entirely within hot28, and their social coupling is expressed at the same threshold. Row/Attached blocks split evenly between hot26 and hot28. Zone 3 therefore represents a structural shift into the extreme regime where social vulnerability (older adults) and compact or perimeter forms coincide.

Microclimatic conditions confirm this severity. UTCI averages 35 to 36°C across the day. PET reaches 41.5°C at 10:00, drops to 39.5°C at 12:00, and returns to 41.6°C at 14:00. At both 10:00 and 14:00, most cases (30/36) exceed 41°C, with a maximum at POI 2 at 14:00 (PET 43.4°C, UTCI 37.0°C, Tmrt 65.8°C). The hottest patches align with high integration corridors, particularly POI 2, 3 and 6, reinforcing convergence between socially sensitive groups, dense morphologies and heavily used pedestrian routes.

Cross case synthesis. The three cases indicate a gradient in how vulnerability is activated across thresholds. In Case 1 (Hospital General), vulnerability is concentrated in the moderate heat band (26 to 28°C), affects all typologies, and is most strongly associated with older adults and low education. In Case 2 (Airport), moderate stress remains dominant, but some morphologies (Low Perimeter and Row/Attached) begin to show hot28 signals that are again tied to educational disadvantage. In Case 3 (Basílica), vulnerability emerges mainly under $\geq 28^\circ\text{C}$, centred on older adults and embedded in compact and perimeter morphologies that intensify exposure.

Across all sites, thermal stress peaks at 14:00 and hotspots align with highly integrated pedestrian

corridors, meaning that the most accessible routes are often also the most exposed. Blocks with Ta in the 26 to 28°C band can still produce Tmrt above 60°C and PET above 41°C, demonstrating why Ta alone underestimates street level risk. Overall, the evidence points to a dual risk in which limited adaptive capacity coincides spatially with urban forms and networks that favour extreme exposure. The implication is a need for differentiated interventions, including continuous shade and cooling refuges on integrated corridors, and targeted programmes for older adults and educationally disadvantaged populations, tuned to whether areas operate under moderate or extreme thermal regimes.

5. Discussion

This study sought to move from surface proxies to lived exposure, and from citywide averages to block and corridor scale analysis in Mexico City. Three findings merit emphasis.

First, Tmrt, rather than LST, governs pedestrian heat stress during hot daytime hours under Mexico City's high elevation and relatively dry air conditions. This aligns with urban biometeorology: SOLWEIG/UMEP resolves short and long wave fluxes and indicates that Tmrt captures the dominant radiative load experienced by pedestrians in complex street canyons (Lindberg et al., 2008; Lindberg and Grimmond, 2011). In the case studies, blocks with air temperature (Ta) in the 26 to 28°C band still produced Tmrt above 60°C and PET above 41°C. This shows why LST or Ta alone can underestimate street level risk and why design targets should be framed against biometeorological, not purely surface, metrics.

Second, exposure is unequal and socially structured. The macro analysis shows strong co-location between hotter blocks ($\geq 26^\circ\text{C}$; $\geq 28^\circ\text{C}$) and socially sensitive groups such as older adults, people with disabilities and carless households, with borough-heterogeneous associations. This pattern mirrors international evidence of systematic disparities in urban heat exposure by social vulnerabilities (Hoffman et al., 2020; Hsu et al., 2021; Krenz and Amann, 2025). Global health monitoring further reports steep rises in heat related mortality and labour losses, which disproportionately affect disadvantaged groups (Romanello et al., 2025; World Health Organization, 2024).

Third, two reinforcing mechanisms translate morphology and networks into lived heat. Structural heat concentrates in compact, sealed fabrics: higher GSI correlates with lower NDVI and higher Ta, and typologies such as dense perimeter blocks and continuous compact forms concentrate risk, consistent with Space Matrix theory on how intensity and coverage modulate sky view and evapotranspiration (Berghauer Pont and Haupt, 2020). Corridor heat emerges where Space Syntax centralities peak: highly integrated, high through movement corridors systematically coincide with hotter segments. This helps explain why least angle pedestrian spines can concentrate both flows and exposure (Hillier and Hanson, 1984; Hillier et al., 2012).

These findings answer the research questions directly: the co location of heat and social sensitivity under locally relevant thresholds confirms that risk is geographically patterned (Q1); hotspot clusters are best characterised by couplings between form and network (Q2); and micro scale simulations show that radiative peaks concentrate on highly integrated corridors, converting remote sensing signals into actionable street segments (Q3).

The policy implication is that heat adaptation should be reframed around measurable outcomes. A Key Performance Indicator (KPI) is a quantifiable metric linked to a specific objective (Parmenter, 2015). In this context, generic outputs such as the number of trees planted are weak substitutes for outcome oriented KPIs that track cooling delivered where people walk and dwell. Suitable KPIs for Mexico City could include:

- Median midday Tmrt reductions of 10 to 15°C along priority corridors
- Continuous shade over at least 70% of pedestrian length between 10:00 and 14:00
- Provision of cooling refuges every 300 to 500 m
- Reduction of hot segment length ($\text{Ta} \geq 28^\circ\text{C}$ at p90)

These indicators can be derived from local and low-cost data such as Landsat imagery, open building footprints, census statistics and simple microclimate modelling, and can support learn-as-you-go governance with feedback loops.

The strategic rationale is twofold. First, passive cooling through shade, ventilation and non glare cool materials reduces cooling demand, limits dependence on energy intensive air conditioning, and mitigates energy poverty risks under warming. International assessments emphasise that reducing emissions from cooling depends on passive design, efficiency and refrigerant transition, with passive measures critical because they reduce demand before efficiency improves use (United Nations Environment Programme, 2023). In Latin America, where energy poverty is a pressing concern, heat resilient public space can directly lower the energy burden of low income households (González and Ibáñez-Martín, 2023). Second, maladaptation risks are material. Reflective pavements may reduce surface temperatures but increase Tmrt for pedestrians at midday if implemented without shading. The Phoenix Cool Pavement pilot reported higher noontime Tmrt on high albedo coatings relative to asphalt (City of Phoenix Street Transportation Department, 2024). The IPCC likewise warns that poorly specified measures can shift or amplify risks and calls for robust monitoring and evaluation frameworks (IPCC, 2022).

Methodologically, the paper demonstrates a city to street pipeline that combines calibration of satellite and ground data, spatially explicit social sensitivity, coupling of form and network, and micro scale biometeorology to produce decision ready KPIs for corridor based interventions. This bridges big data screening and site specific design and aligns with programmes that move from action lists to performance tracked delivery (ETH Zürich and Singapore, 2017; World Bank, 2025). Limitations remain, including a focus on midday calibration, uncertainty in emissivity estimates derived from NDVI, topology effects on syntax metrics, simplified UMEP assumptions that exclude anthropogenic heat, and socio-demographic variables that act as proxies rather than direct measures of exposure. Nonetheless, triangulation across macro, meso and micro scales yields consistent patterns with clear operational implications.

6. Conclusions

This study set out to translate urban heat from a surface proxy into an account of lived exposure on Mexico City's streets. Addressing this required a multi scalar framework. A decadal summer climatology, calibrated with Landsat 8/9 and RedMet observations, was integrated with configurational, morphological and census based metrics to identify thermo social hotspots where thermal intensity and social vulnerability coincide. The resulting workflow shifts emphasis from surface cartography towards an operational basis for targeted urban intervention.

Three findings stand out:

1. Under conditions of high irradiance and relatively dry air, **mean radiant temperature (Tmrt)**, rather than **land surface temperature (LST)** or **air temperature (Ta)**, governs pedestrian heat stress at midday. Design targets therefore need to be anchored in biometeorological, not solely surface, metrics (Lindberg et al., 2008; Jendritzky et al., 2012).
2. By combining thermal layers with Space Syntax, Space Matrix and socio-demographic predictors, **exposure becomes concrete**. High flow corridors without shade, and morphological types such as dense perimeter and compact low rise, emerge as areas where heat and disadvantage converge (Hillier and Hanson, 1984; Hillier et al., 2012; Berghaus Pont and Haupt, 2020).
3. The **thermo-social hotspot approach** ensures that priorities for adaptation are located precisely where thermal risk and vulnerability coincide in statistically significant ways.

The contribution is twofold. Substantively, the analysis demonstrates that **thermal justice is spatially patterned**: the corridors and neighbourhoods where heat and social disadvantage coincide follow urban and social structures rather than random distributions. Methodologically, it provides a **replicable bridge** from metropolitan screening to microclimatic street scale simulation using open tools (Google Earth Engine, DepthmapX, UMEP/QGIS), enabling multi level interventions that connect evidence and design practice.

The framework also connects to a global challenge. Rising temperatures are driving rapidly increasing demand for cooling. The International Energy Agency projects that, without efficiency measures, electricity use for space cooling will triple by 2050, with steep demand peaks in emerging economies (International Energy Agency, 2018). At the same time, reliance on air conditioners and fans can create an urban vicious circle: extreme heat increases device use, condensers expel residual heat into the street, nocturnal air temperatures rise in dense districts by up to 1 to 2°C, and demand increases again the following day (Sailor, 2014; Salamanca et al., 2014; Santamouris, 2016).

In this context, passive solutions have strategic value. While the transition to cleaner and more efficient technologies remains essential, shade, vegetation and cool materials are irreplaceable in public space. Streets that lower Tmrt, provide continuous shade and ensure accessible refuges can protect health, relieve pressure on electricity grids and mitigate energy poverty (Khosla et al., 2021; United Nations Environment Programme, 2023).

In sum, the paper moves beyond mapping heat by translating urban science into actionable goals that cool streets, reduce network loads and protect those least able to afford mechanical cooling. The results indicate that effective urban adaptation depends on solutions that cool without warming the city further, and they motivate a programme of research action to cool, equitably and sustainably, the streets that need it most in Mexico City.

Reference

References

- Berghauer Pont, M. and Haupt, P. (2020), *Spacematrix: Space, Density and Urban Form*, 2nd edn, nai010 publishers, Rotterdam. doi: 10.59490/mg.38.
- Bröde, P., Fiala, D. et al. (2012), ‘Derivation and validation of the universal thermal climate index (UTCI)’, *International Journal of Biometeorology* **56**, 481–494. doi: 10.1007/s00484-011-0454-1.
- Chakraborty, T. et al. (2022), ‘Lower urban humidity moderates outdoor heat stress’, *AGU Advances* **3**(4), e2022AV000729. doi: 10.1029/2022AV000729.
- City of Phoenix Street Transportation Department (2024), Cool pavement program – phase II report, Technical report, City of Phoenix, Phoenix, AZ.
https://www.phoenix.gov/content/dam/phoenix/streetssite/documents/cool-pavement/CoolPavement_Phase2_Report_FINALOct24.pdf
- de Foy, B., Fast, J. D., Paech, S. J. et al. (2006a), ‘Distinct wind convergence patterns in the Mexico City basin due to the interaction of gap winds with the synoptic flow’, *Atmospheric Chemistry and Physics* **6**, 1249–1265. doi: 10.5194/acp-6-1249-2006.
- de Foy, B., Fast, J. D., Paech, S. J. et al. (2006b), ‘Rapid ventilation of the Mexico City basin and regional fate of the urban plume’, *Atmospheric Chemistry and Physics* **6**, 2321–2335. doi: 10.5194/acp-6-2321-2006.
- ETH Zürich and Singapore (2017), Strategies for cooling singapore: A catalogue of urban heat mitigation measures, Technical report, ETH Zürich / Singapore-ETH Centre, Singapore. doi: 10.3929/ethz-b-000258216.
- González, F. A. I. and Ibáñez-Martín, M. M. (2023), ‘Six decades of energy poverty: Reducing disparities in Latin America and the Caribbean?’, *Revista INVI* **38**(109), 71–99. doi: 10.5354/0718-8358.2023.70125.
- Google Research (2023), ‘Open buildings v3 (Latin America extension)’. Accessed: 13 May 2025.
<https://sites.research.google/open-buildings/>
- Gorelick, N. et al. (2017), ‘Google Earth Engine: Planetary-scale geospatial analysis for everyone’, *Remote Sensing of Environment* **202**, 18–27. doi: 10.1016/j.rse.2017.06.031.
- Hillier, B. and Hanson, J. (1984), *The Social Logic of Space*, Cambridge University Press, Cambridge. doi: 10.1017/CBO9780511597237.
- Hillier, B., Yang, T. and Turner, A. (2012), ‘Normalising least angle choice in Depthmap and how it opens up new perspectives on the global and local analysis of city space’, *Journal of Space Syntax* **3**(2), 155–193.
<http://joss.bartlett.ucl.ac.uk/journal/>
- Hoffman, J. S., Shandas, V. and Pendleton, N. (2020), ‘The effects of historical housing policies on resident exposure to intra-urban heat: A study of 108 US urban areas’, *Climate* **8**(1), 12. doi: 10.3390/cli8010012.
- Hsu, A. et al. (2021), ‘Disproportionate exposure to urban heat island intensity across major US cities’, *Nature Communications* **12**, 2721. doi: 10.1038/s41467-021-22799-5.
- Höppe, P. (1999), ‘The physiological equivalent temperature (PET)—a universal index for the biometeorological assessment of the thermal environment’, *International Journal of Biometeorology* **43**, 71–75. doi: 10.1007/s004840050119.

- INEGI (2021), 'Censo de población y vivienda 2020: Resultados por AGEB y manzana urbana'. Accessed: 31 May 2025.
<https://www.inegi.org.mx/programas/ccpv/2020/>
- International Energy Agency (2018), The future of cooling: Opportunities for energy-efficient air conditioning, Technical report, IEA, Paris.
<https://www.iea.org/reports/the-future-of-cooling>
- International Labour Organization (2019), Working on a warmer planet: The impact of heat stress on labour productivity and decent work, Technical report, ILO, Geneva.
- IPCC (2022), Climate change 2022: Impacts, adaptation and vulnerability, in 'Working Group II Contribution to the Sixth Assessment Report', Cambridge University Press, Cambridge, pp. 3–33. doi: 10.1017/9781009325844.001.
- Jendritzky, G., de Dear, R. and Havenith, G. (2012), 'UTCI—why another thermal index?', *International Journal of Biometeorology* **56**, 421–428. doi: 10.1007/s00484-011-0453-2.
- Jáuregui, E. (1997), 'Heat island development in Mexico City', *Atmospheric Environment* **31**(22), 3821–3831. doi: 10.1016/S1352-2310(97)00136-2.
- Khosla, R. et al. (2021), 'Cooling for sustainable development', *Nature Sustainability* **3**, 201–208. doi: 10.1038/s41893-020-00627-w.
- Krenz, K. and Amann, L. (2025), 'Urban heat island effect: examining spatial patterns of socio-demographic inequalities in Greater London', *Buildings and Cities* pp. 1–25. doi: 10.1080/23748834.2025.2489854.
- Lavell, A. (1999), *Gestión de riesgos ambientales urbanos*, LA RED / FLACSO, San José.
<https://www.desenredando.org/>
- Lavell, A. (2003), *Conceptos y definiciones básicas para la gestión del riesgo*, CLACSO, Buenos Aires.
- Liang, S. (2001), 'Narrowband to broadband conversions of land surface albedo I: Algorithms', *Remote Sensing of Environment* **76**(2), 213–238. doi: 10.1016/S0034-4257(00)00205-4.
- Lindberg, F. and Grimmond, C. S. B. (2011), 'The influence of vegetation and building morphology on shadow patterns and mean radiant temperature in urban areas', *Theoretical and Applied Climatology* **105**, 311–323. doi: 10.1007/s00704-010-0382-8.
- Lindberg, F., Holmer, B. and Thorsson, S. (2008), 'SOLWEIG 1.0—modelling spatial variations of 3D radiant fluxes and mean radiant temperature in complex urban settings', *International Journal of Biometeorology* **52**, 697–713. doi: 10.1007/s00484-008-0162-7.
- Lindberg, F. et al. (2018), 'UMEP—an integrated tool for urban climatology in QGIS', *Environmental Modelling & Software* **99**, 70–87. doi: 10.1016/j.envsoft.2017.09.020.
- Magaña, V. and Vargas, N. (2020), 'Warm spells and climate risk to human health in the Mexico City Metropolitan Area', *Weather, Climate, and Society* **12**(3), 351–365. doi: 10.1175/WCAS-D-19-0096.1.
- Matzarakis, A., Mayer, H. and Iziomon, M. G. (1999), 'Applications of a universal thermal index: PET', *International Journal of Biometeorology* **43**, 76–84. doi: 10.1007/s004840050118.
- Matzarakis, A., Rutz, F. and Mayer, H. (2007), 'Modelling radiation fluxes in simple and complex environments', *International Journal of Biometeorology* **51**, 323–334. doi: 10.1007/s00484-006-0061-8.
- NASA (2025), 'Temperatures rising: NASA confirms 2024 warmest year on record'.
<https://www.nasa.gov/news-release/temperatures-rising-nasa-confirms-2024-warmest-year-on-record/>
- NOAA (2025), 'Global climate report—annual 2024'.
<https://www.ncei.noaa.gov/access/monitoring/monthly-report/global/202413>
- Parmenter, D. (2015), *Key Performance Indicators: Developing, Implementing, and Using Winning KPIs*, 3rd edn, Wiley, Hoboken, NJ.
- Rohde, R. A. (2025), 'Global temperature report for 2024'.
<https://berkeleyearth.org/global-temperature-report-for-2024/>
- Romanello, M. et al. (2025), 'The 2025 report of the Lancet Countdown on health and climate change: climate change action offers a lifeline', *The Lancet* **406**(10521), 2804–2857. doi: 10.1016/S0140-6736(25)01919-1.
[https://www.thelancet.com/journals/lancet/article/PLIIS0140-6736\(25\)01919-1/fulltext](https://www.thelancet.com/journals/lancet/article/PLIIS0140-6736(25)01919-1/fulltext)

- Sailor, D. J. (2014), 'Risks of summertime extreme thermal conditions in buildings as a result of climate change and exacerbation of urban heat islands', *Building and Environment* **78**, 81–88. doi: 10.1016/j.buildenv.2014.04.012.
- Salamanca, F. et al. (2014), 'Anthropogenic heating of the urban environment due to air conditioning', *Journal of Geophysical Research: Atmospheres* **119**(10), 5949–5965. doi: 10.1002/2013JD021225.
- Santamouris, M. (2016), 'Innovating to zero the building sector in Europe: Minimising the energy consumption, eradication of the energy poverty and mitigating the local climate change', *Solar Energy* **128**, 61–94. doi: 10.1016/j.solener.2016.01.021.
- SEDEMA (2021), Estrategia local de acción climática 2021–2050 y programa de acción climática 2021–2030, Technical report, Government of Mexico City, Mexico City.
<http://www.data.sedema.cdmx.gob.mx/cambioclimaticocdmx/>
- Stewart, I. D. and Oke, T. R. (2012), 'Local climate zones for urban temperature studies', *Bulletin of the American Meteorological Society* **93**(12), 1879–1900. doi: 10.1175/BAMS-D-11-00019.1.
- Tucker, C. J. (1979), 'Red and photographic infrared linear combinations for monitoring vegetation', *Remote Sensing of Environment* **8**(2), 127–150. doi: 10.1016/0034-4257(79)90013-0.
- United Nations Environment Programme (2023), Global cooling watch: Keeping it chill, Technical report, UNEP, Nairobi. doi: 10.59117/20.500.11822/44243.
- Waleed, M. et al. (2023), 'Towards sustainable and livable cities: Leveraging remote sensing, machine learning, and geo-information modelling to explore and predict thermal field variance in response to urban growth', *Sustainability* **15**(2), 1416. doi: 10.3390/su15021416.
- World Bank (2025), Shaping a cooler Bangkok: Heat action plan and investment priorities, Technical report, World Bank, Bangkok.
<https://documents1.worldbank.org/>
- World Health Organization (2024), Heat and health, Technical report, WHO, Geneva.
<https://www.who.int/news-room/fact-sheets/detail/climate-change-heat-and-health>
- World Meteorological Organization (2025), State of the global climate 2024, Technical report, WMO, Geneva.
https://wmo.int/sites/default/files/2025-03/WMO-1368-2024_en.pdf
- Zha, Y., Gao, J. and Ni, S. (2003), 'Use of normalized difference built-up index in automatically mapping urban areas from TM imagery', *International Journal of Remote Sensing* **24**(3), 583–594. doi: 10.1080/01431160304987.